ACS OMEGA

Open Access

http://pubs.acs.org/journal/acsodf

Article

Ternary Blends of Polypropylene Copolymer, Polyethylene and Thermoplastic Polyurethane for Fused Deposition Modeling Three-Dimensional Printing Technology: Preparation, Printing and Properties

Wasana Kosorn,[#] Pornchanok Pichaipanich,[#] Phansiri Suktha, Nutdanai Nampichai, Boonlom Thavornyutikarn,* and Wanida Janvikul*

Cite This: *ACS Omega* 2024, 9, 35131−35143

Read Online

ACCESS | Metrics & More | Article Recommendations | Supporting Information

ABSTRACT: A set of filaments for fused deposition modeling (FDM) three-dimensional (3D) printing was developed from the ternary blends of polypropylene random copolymer (PPR or P), high density polyethylene (HDPE or E), and thermoplastic polyurethane (TPU or T), formulated with different weight ratios of polymers, i.e., 80:20:0, 70:20:10, 60:20:20, and 50:20:30, respectively, and coded as P80E20T0, P70E20T10, P60E20T20, and P50E20T30, respectively. The blend composition was optimized to obtain both high-quality filaments with low ovality and FDM-fabricated objects with minimized warpage and good interlayer bonding. The crystallization and crystalline morphologies of individual polymers in the blend filaments were comprehensively analyzed by differential scanning calorimetry (DSC), X-ray diffraction (XRD), and polarized light optical microscopy (PLOM). It was found that HDPE acted as crystalline nuclei for PPR crystallization; PPR appeared to crystallize more readily at a slightly higher T_c with somewhat greater crystallinity. Meanwhile, TPU explicitly restricted the crystallization of both polyolefins; decreases in both the size and growth rate of their spherulites were observed. The PLOM and SEM results indicated that the surface morphology of the ternary blends was not absolutely phase-separated; an increasing number of TPU droplets inherently imbedded at the boundary of the polyolefin aggregate phase when a higher TPU quantity was integrated. Consequently, the warpage deformation and layer interfusion of the as-printed articles were most remarkably improved when P50E20T30 was used. Nonetheless, the incorporation of relatively flexible TPU material into the PPR-based filaments inevitably reduced their mechanical performance; the flexural strength and modulus of the highest-quality 3D-printed P50E20T30 object were fairly decreased by approximately 25% and 12%, respectively.

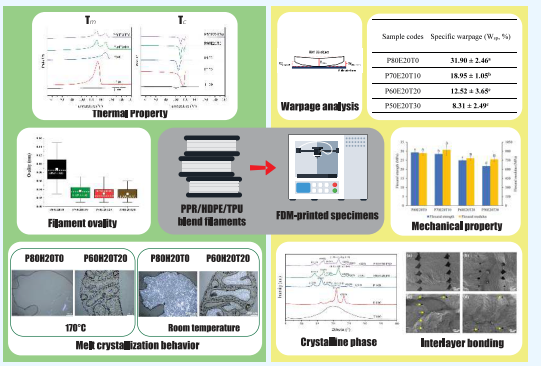

1. INTRODUCTION

Fused deposition modeling (FDM) is a three-dimensional (3D) printing technique that has been extensively exploited in academic R&D and industrial work owing to its ease to use and ready availability of machines at low cost.[1,2] Despite such advantages, one of the major constraints for developing FDM-printed specimens with desirable properties for high-performance applications is the limited availability of commercial FDM printing feedstocks. Most substantially used FDM materials are polymers, particularly amorphous thermoplastic polymers such as polylactic acid, acrylonitrile butadiene styrene copolymer, polyurethane, and polycarbonate.[3] A smaller number of semicrystalline thermoplastic filaments are commercially available for FDM printing.

Such semicrystalline thermoplastic materials as polyolefins, i.e., polypropylene (PP) and polyethylene (PE), are commonly exploited in daily life in a wide variety of applications. PP is one of the most produced and consumed thermoplastics as a result of its chemical and biological inertness, low density, ease of processing, recyclability, and relatively low cost.[4] Due to these benefits, the fabrication of PP-based objects by means of FDM 3D printing has increasingly attracted attention from related users.[5−8] However, the crystallization of PP leads to anisotropic behavior, causing thermal shrinkage and warpage during the cooling process of the molten material. This phenomenon thus affects the bonding between adjacent filament strands, the fusion of layers, and the adhesion of deposited layers onto standard build plates such as glass mirrors.[9] A series of papers by Spoerk et al.[10,11] has confirmed

Received: June 12, 2024
Revised: July 17, 2024
Accepted: July 23, 2024
Published: August 1, 2024

that the lack of layer adhesion primarily resulted from warpage, delamination of the first layer, and an unfavorable build platform temperature. High density polyethylene (HDPE) is another most supplied and used thermoplastic; it has been extensively employed in biomedical applications because of its inertness and good mechanical properties.[12] In recent years, several research studies have been explored to boost its use in FDM printing.[13−15] The FDM printing of neat HDPE filament has, however, been scarcely successful due to crystallization-induced volume contraction, resulting in poor bed adhesion and specimen shrinkage during the printing process. These apolar polymers explicitly exhibit poor adhesion to most FDM platform surfaces. Blending such semicrystalline polyolefins with other polymers is an efficient and cost-effective approach to overcome their warpage and interlayer strength problems occurring during FDM printing.[16] For instance, the study of Peng et al.[17] demonstrated that FDM printing of blend filaments of isotactic polypropylene (iPP) and nylon-6 resulted in the 3D specimens with markedly enhanced dimensional stability and appropriate mechanical properties. Another study by Slonov et al.[18] also revealed that blending HDPE with ethylene-vinyl acetate copolymer (up to 70 wt %) distinctly improved the processability and printability of the developed HDPE-based filaments.

Recently, attempts to blend polyolefins with thermoplastic elastomers (TPEs) have been explored for development of high-performance FDM filaments and 3D-printed objects[19,20] as TPEs possess unique elasticity and thermoplastic-like processability. The study of Ho et al.[20] reported that the addition of elastomeric ethylene-octene copolymer (20−40 wt %) in the iPP filament matrix increased the flow property and the interfacial fusion between the printed layers, resulting in the FDM-fabricated specimens with improved mechanical properties. Banerjee et al.[21] developed the 3D-printable materials from iPP blended with styrene-(ethylene-butylene)-styrene block copolymers (SEBS) (20−80 wt %). The 3D-printed iPP/SEBS specimens exhibited good thermoplastic elastomeric behavior. Lately, new FDM composite filaments have been developed from the mixed powders of iPP (about 5 wt %), thermoplastic polyurethane (TPU), and barium titanate ($BaTiO_3$).[22] The PP/TPU filament integrated with 35 wt % $BaTiO_3$ appeared to be the most readily printed material; no clogging of the nozzle and no troubles with multilayer deposition were reported. Absolutely, adding iPP into the TPU-based composites could intervene in the entire morphology of the composite matrices; however, this could be rather difficult to observe because of the minimal content of iPP combined.

In general, a semicrystalline polymer forms densely packed and organized crystalline regions upon cooling. It is of importance to thoroughly understand the crystalline behavior of a newly developed polymer blend filament based on semicrystalline polyolefins, which is essentially a prerequisite for FDM printing. In this present work, we report, for the first time, on the development of high-performance FDM filaments from the ternary blends of two different semicrystalline polyolefins, i.e., polypropylene random copolymer (PPR) and HDPE, and TPU. A melt-mixing method was employed for the preparation of a series of high-performance PPR/HDPE/TPU ternary blend filaments containing 0−30 wt % TPU. The physical and thermal properties of the prepared blend filaments were comparatively evaluated in terms of filament ovality, phase morphology, crystallinity, and crystallization behaviors. The as-printed objects obtained from these developed blend filaments were also comparatively assessed in terms of warpage deformation, surface morphology, and mechanical properties.

2. EXPERIMENTAL PROCEDURES

2.1. Materials. Polypropylene random copolymer (PPR) with a melt flow rate (MFR) of 8 g/10 min at 230 °C was purchased from HMC polymers, Thailand. High density polyethylene (HDPE) with an MFR of 0.04 g/10 min at 190 °C was obtained from PTT Global Chemical, Thailand. Thermoplastic polyurethane (TPU) with MFR of 56 g/10 min at 210 °C and a shore hardness of 92A (DIN ISO 7619−1) was bought from Covestro AG, Thailand. According to the technical data sheets, the flexural moduli of PPR and HDPE were 1030 MPa (ASTM D790A) and 1177 MPa (ASTM D790), respectively.

2.2. Fabrication of PPR/HDPE/TPU Blend Filaments. In this study, PPR (concisely encoded as P) was used as the main filament matrix. HDPE (shortly encoded as E) was combined into the individual blend filaments at the fixed weight percentage (20 wt %), and TPU (briefly encoded as T) was integrated into the blends at varied weight percentages (0−30 wt %). At first, TPU pellets were primarily dried overnight in a convection oven at 80 °C to remove any moisture trapped in the pellets before being blended with PPR and HDPE at various weight ratios of P:E:T, i.e., 80:20:0, 70:20:10, 60:20:20, and 50:20:30, to generate the PPR-based blend filaments designated as P80E20T0, P70E20T10, P60E20T20, and P50E20T30, respectively, as summarized in Table 1.

Table 1. Compositions of the Developed PPR-Based Blend Filaments

Filament codes	PPR (wt %)	HDPE (wt %)	TPU (wt %)
P80E20T0	80	20	0
P70E20T10	70	20	10
P60E20T20	60	20	20
P50E20T30	50	20	30

The preparation process of the PPR-based blend filaments is depicted in Scheme 1a. The blend filaments were individually fabricated by a melt-blending method using a modular 16 mm twin-screw extruder, having a 3 mm die nozzle and equipped with a filament production line (LTE16-40, Labtech Engineering Co., Ltd., Samut Prakan, Thailand). The optimum barrel temperatures were set at 195−210 °C while the die temperature of the gear pump was set at 195−200 °C. The speed of screw rotation was set at 200−250 rpm. Each polymer blend was extruded through a die into a water bath set at 80 °C with a pulling speed in the range of 11.5−12.4 m/min to form a rod-shaped filament and eventually wound up with a filament rolling system on a spool. The extrusion process of each blend was optimized to ensure the achievement of a high-quality blend filament. The diameter of each fabricated filament was regularly checked at every 50 cm length by using a digital caliper. The ovality of each extruded filament was determined using eq 1; the lengths of the maximum and minimum axes of the cross-sectional area of each extruded filament at 20 randomly selected points of the filament were measured using a digital caliper micrometer.[23]

$$\text{Ovality} = \text{maximum diameter} - \text{minimum diameter} \quad (1)$$

https://doi.org/10.1021/acsomega.4c05502
ACS Omega 2024, 9, 35131−35143

Scheme 1. Schematic Illustrations of (a) the Preparation of the 3D Printing PPR-Based Blend Filaments and (b) the FDM Fabrication of the PPR-Based Blend Specimens

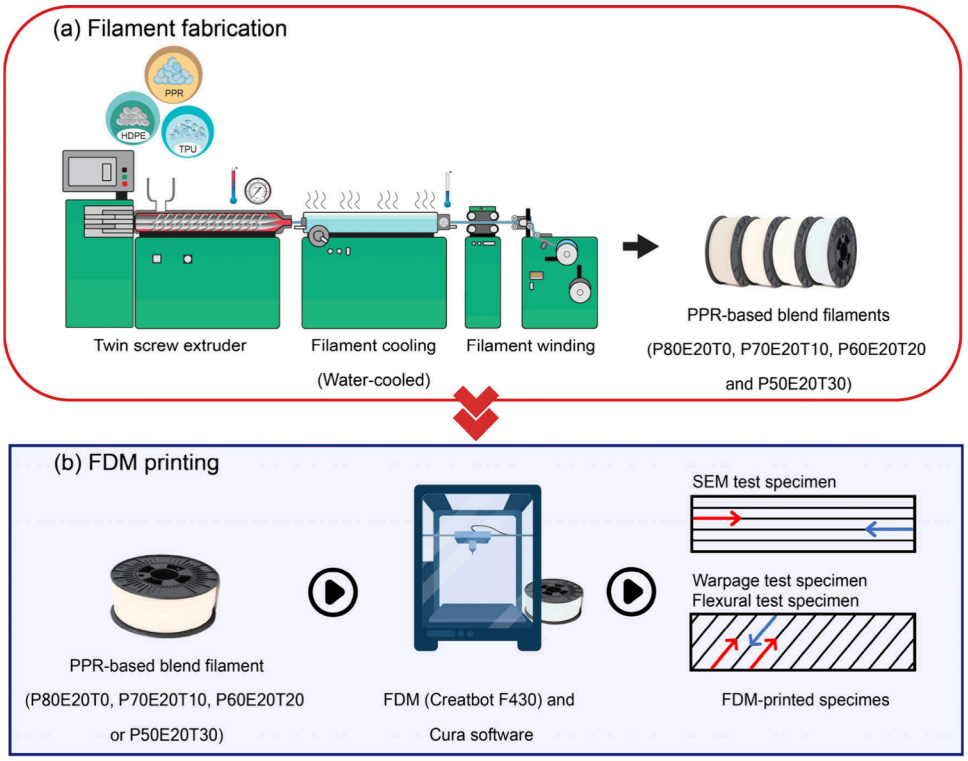

2.3. FDM Printing of PPR-Based Blend Filaments. The 3D printing of each PPR/HDPE/TPU blend filament was carried out by using an FDM 3D printer (Creatbot F430, Henan, China) with a carbon fiber printing bed, as illustrated in Scheme 1(b). The Cura software (Ultimaker, Geldermalsen, The Netherlands) was used to export the 3D models in STL files to G-code. Table 2 displays a list of the optimized FDM printing parameters for fabrication of the 3D PPR-based blend objects. The raster angle of 45°/−45° was principally used in the fabrication of 3D test specimens, unless otherwise stated.

Table 2. Summary of Process Parameters for the FDM-Printing of the PPR-Based Blend Filaments

Parameters	Values
Nozzle temperature (°C)	220
Printing bed temperature (°C)	100
Nozzle diameter (mm)	1.0
Layer thickness (mm)	0.25
Printing speed (mm/s)	30
Print infill (%)	100
Raster angle	0, 45°/−45°
Chamber temperature (°C)	50

2.4. Characterizations of PPR-Based Blend Filaments. *2.4.1. Differential Scanning Calorimetry (DSC).* A differential scanning calorimeter (*Mettler Toledo DSC 822e, USA*) was used in the evaluation of the thermal properties of the individual extruded blend filaments, i.e., melting temperature (T_m), crystallization temperature (T_c), and degree of crystallinity (X_c). The thermal properties of the starting pristine polymers were also comparatively determined. In brief, approximately 10 mg of each sample were placed in a sealed DSC aluminum pan. Each DSC analysis was then conducted with two heating cycles from −80 to 240 °C at a rate of 10 °C/min and one intermediate cooling cycle from 240 °C to −80 °C at a rate of 10 °C/min. All measurements were performed under a nitrogen atmosphere. The melting behavior and degree of crystallinity of each test material were analyzed by using the Universal analysis software. The melting endotherms of the second heating scans were employed for the determinations of crystalline melting points, heat of fusion (or melting enthalpy (ΔH_m) which was directly governed by the area(s) underneath the melting peak(s)), and degrees of crystallinity of the individual test materials. The percent crystallinity ($\%X_c$) was calculated by using eq 2[9] with some modifications.

$$\%X_c = \left(\frac{\Delta H_m}{[\Delta H_{m,0} * x] + [\Delta H'_{m,0} * y] + [\Delta H''_{m,0} * z]} \right) \times 100 \quad (2)$$

where ΔH_m is the melting enthalpy of a test material (J/g) analyzed by DSC. $\Delta H_{m,o}$, $\Delta H'_{m,o}$ and $\Delta H''_{m,o}$ are the melting enthalpies of the completely crystalline PPR, HDPE and TPU, respectively. In this study, the melting enthalpy of 100% crystalline isotactic polypropylene (iPP) (207 J/g)[24] was used for $\Delta H_{m,o}$. $\Delta H'_{m,o}$ of 100% crystalline HDPE was previously reported to be 293 J/g[25] while $\Delta H''_{m,o}$ of the crystalline TPU was found to be 196.8 J/g.[26] The variables x, y, and z correspond to the weight fractions of PPR, HDPE, and TPU, respectively, in the ternary blends.

The theoretical percent crystallinity ($\%X_{c,theo}$) of the PPR-based blends were also calculated using eq 3.

$$\%X_{c,theo} = (X_{c,PPR} * x) + (X_{c,HDPE} * y) + (X_{c,TPU} * z) \quad (3)$$

https://doi.org/10.1021/acsomega.4c05502
ACS Omega 2024, 9, 35131−35143

where $X_{c,PPR}$, $X_{c,HDPE}$, and $X_{c,TPU}$ are the degrees of crystallinity of the pristine PPR, HDPE, and TPU samples, respectively, determined directly from their DSC thermograms, and the variables x, y, and z correspond to the weight fractions of PPR, HDPE, and TPU, respectively, in the blends.

2.4.2. Hot Stage Polarized Light Optical Microscopy (PLOM). The crystalline morphologies of both pristine and blended polymers were comparatively examined by using a polarized light optical microscope (BX53, Olympus, Japan) equipped with a hot stage. In brief, both PPR-based blend filaments and neat polymer pellets were sectioned into slices with a thickness of approximately 5 μm using a microtome (EMFCS, Leica). Slices of individual materials were placed between a glass slide and a coverslip and subsequently heated at 240 °C for 4 min before being cooled at a rate of 10 °C/min to certain temperatures, e.g., 170 °C, 160 °C and 150 °C, at which the specimens were held still for 5 min. To observe the crystalline morphologies of PPR, HDPE and TPU in the neat pellets and blend filaments, the specimens were further cooled to the isothermal temperatures of 150 °C for TPU, 120 °C for HDPE, and 110 °C for PPR and held at the constant temperatures for varied times, e.g., 5, 10, 20, and 60 min before observation. The microscope was controlled by the cellSens Standard software (Olympus, Japan); each set of PLOM micrographs was recorded at a magnification of 5x during the entire crystallization process.

2.4.3. Scanning Electron Microscopy (SEM). To examine the fractured surface microstructures of the PPR-based blend filaments, the filament specimens were broken under liquid nitrogen, gold-sputtered, and then investigated by a field emission scanning electron microscope (FE-SEM, HITACHI/SU5000, Japan). The SEM images were taken at an accelerating voltage of 5 kV.

2.5. Characterization of 3D-Printed Blend Specimens.

2.5.1. X-ray Diffraction (XRD) Analysis. An X'Pert Pro Powder Diffractometer (Malvern PANalytical, UK), equipped with a copper radiation source (CuKα, λ = 0.1542 nm), was employed to obtain the XRD patterns of the PPR-based blend and parent polymer specimens. The PPR-based blend specimens with dimensions of 8 mm width, 8 mm length, and 2 mm thickness were fabricated from the individual PPR-based blend filaments using the FDM-printing parameters tabulated in Table 2, whereas the disc specimens (7 mm diameter and 1 mm thickness) of the pristine polymer specimens were prepared by pressing the polymer pellets at ambient temperature. The XRD analysis was performed by using the following conditions: 40 kV, 30 mA, angular range (2θ) of 5°−40°, and scanning rate of 2°/min. The degree of crystallinity of each test material was promptly determined from a ratio of the peak areas of the crystalline phase to the sum of the areas of the crystalline and amorphous phases (the total surface area under the XRD curve). The baselines of the individual crystalline peaks in the XRD patterns were manually fitted by using OriginPro 2018 (*OriginLab Corporation, USA*).

2.5.2. Assessment of Interlayer Bonding between Layers of 3D-Printed Polymer Blend Objects. The rectangular-shaped specimens (10 mm width × 80 mm length × 3 mm thickness) were printed from the PPR-based blend filaments with a raster angle of 0°. To observe the interlayer bonding between layers of each 3D object (Figure 1), the sample was cryo-fractured using liquid nitrogen, gold-sputtered, and then examined by a field emission scanning electron microscope (FE-SEM, HITACHI/SU5000, Japan). The SEM photographs of the fractured surfaces of the as-printed objects were made at an accelerating voltage of 5 kV.

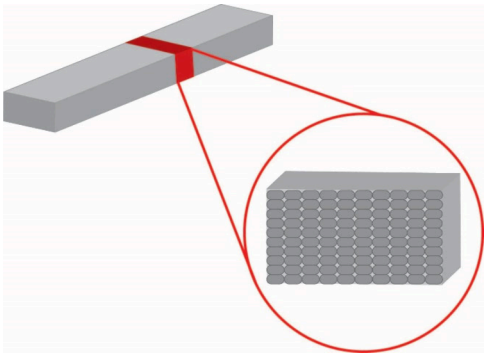

Figure 1. Cryo-fractured surface of a rectangular blend object FDM-printed with a raster angle of 0°.

2.5.3. Warpage Evaluation. To measure warpage deformation of 3D-fabricated specimens, the method reported by Bachhar et al.[27] was employed. Briefly, the 3D specimens (10 mm width × 80 mm length × 4 mm thickness) were fabricated from the individual PPR/HDPE/TPU blend filaments by using the FDM-printing parameters illustrated in Table 2; no adhesive was initially applied on the carbon fiber build platform. The as-printed specimens were left at ambient temperature for 24 h before being photographed. The absolute warpage ($W_{abs,Left}$ and $W_{abs,Right}$) and the maximum height (H_{max}) of each fabricated specimen were subsequently determined from the corresponding photograph using ImageJ software (version 1.54d, National Institutes of Health, Bethesda, MD, USA), as graphically shown in Figure 2. The specific warpage (W_{sp}) of the fabricated specimen was ultimately calculated using eq 4; three different specimens (n = 3) printed from the same blend filament were analyzed.

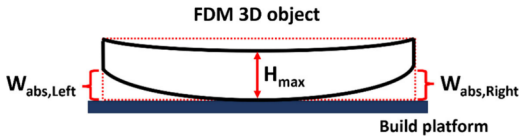

Figure 2. Measurement of warping deformation at the corners of an as-printed object.

$$\text{Specific warpage } (W_{sp}) = \left[\frac{\left(\frac{W_{abs,Left} + W_{abs,Right}}{2}\right)}{H_{max}}\right] \times 100 \quad (4)$$

2.5.4. Mechanical Property Testing. The mechanical performances of the individual FDM-printed specimens (10 mm width × 80 mm length × 4 mm thickness) were determined at room temperature using a Universal Testing Machine (AGX-V, Shimadzu, Japan) in a flexural mode with a crosshead testing rate of 2 mm/min, load capacity of 10 kN, and span length of 64 mm, in accordance with ISO 178.[28] All measurements were repeated at least five times.

2.6. Statistical Analysis. The statistical significances for warpage deformation and mechanical performance of the FDM-printed PPR/HDPE/TPU objects were determined by SPSS software (version 19.0; SPSS, Inc., Chicago, IL) using a one-way analysis of variance (ANOVA) with a Duncan

https://doi.org/10.1021/acsomega.4c05502
ACS Omega 2024, 9, 35131−35143

posthoc test. All data were obtained from quintuplicate experiments, unless otherwise noted, and presented as the mean ± SD. The statistical significance was set at a confidence level of 95% (p-value < 0.05).

3. RESULTS AND DISCUSSION

3.1. Filament Fabrication. Filament uniformity is of importance, as it is a direct indicator of a successful filament fabrication. To ensure steady and continuous printing of FDM feedstocks and no printer clogs, the whole extruded filament has to be consistently round and smooth. In this study, PPR-based blend filaments for FDM printing were prepared from varied blend compositions of PPR, HDPE, and TPU; the blends of three different polymer pellets were individually extruded into continuous filaments with a targeted diameter of 1.75 mm using a twin-screw extruder equipped with a filament production line, as illustrated in Scheme 1a. The maximum and minimum diameters of each fabricated filament were periodically measured at an interval of 50 cm for 20 points using a digital vernier caliper and then averaged. The overall average diameters of the filaments were subsequently calculated. All determined averages of filament diameters are tubulated in Table S1 in the Supporting Information (SI). Apparently, all fabricated PPR-based blend filaments possessed smooth surfaces with overall average diameters in the range of (1.75 ± 0.02)−(1.76 ± 0.05) mm. Such filament uniformity could sufficiently enable a reliable 3D printing process. When the amount of TPU incorporated was increased, not only did the average diameter of the PPR/HDPE/TPU ternary blend filament become closer to 1.75 mm but also the standard deviation turned smaller. The highest average diameter with the greatest standard deviation was apparently observed in the PPR/HDPE binary blend filament (P80H20T0). The incorporation of TPU, which has a relatively low viscosity, readily boosted the flowability of the extruded blended materials during the filament making process.

In this work, the ovality value of each fabricated blend filament was promptly determined from the difference between the maximum and minimum diameters of the filament, which were separately measured at 20 points per filament. Generally, the lower the ovality value is, the rounder the filament becomes.[29] The ovality values of the blend filaments are displayed by a box-and-whisker plot created by OriginPro 2018 (OriginLab Corporation, USA), as shown in Figure 3. In this graph, a box was drawn from the first quartile to the third quartile; hence, the width of the box was used to evaluate the data variation. The whiskers were drawn from each quartile to the minimum or maximum, reflecting the distribution of the ovality values of each filament. The median and mean (average diameter) are also presented as a dashed line and a small square, respectively, in each box. It was noted that both median and whisker length decreased with the increase of TPU content; the average (mean) ovality explicitly dropped from 0.088 ± 0.03 mm to 0.030 ± 0.02 mm. More interestingly, incorporating higher TPU contents into the PPR/HDPE/TPU ternary blends drastically shifted the median values downward to the lower quartile, indicating a closer-to-round shape of the ternary blend filament. This was possibly because the entangled TPU chains restricted the crystallization of PPR and HDPE chains, and then the material shrinkage was minimized. As a result, P50H20T30 exhibited the lowest median.

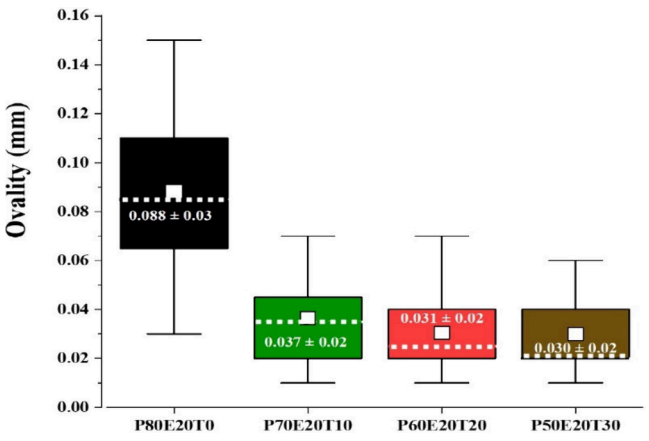

Figure 3. Box-and-whisker plot of the ovality values of the PPR-based blend filaments.

3.2. Thermal Property. The thermal properties of the PPR-based blend filaments incorporated with and without TPU were comparatively examined by differential scanning calorimetry (DSC) with respect to those of the parent polymers. The DSC specimens of P80E20T0 and P50E20T30 were cut from the filaments, while those of the pristine polymers were promptly obtained from the virgin polymer pellets. The DSC thermograms of the heating (second scan) and cooling profiles of each test material are shown in Figure 4, and the measured melting and crystallization temperatures of each polymer are summarized in Table 3. Figure 4a reveals the endothermic melting peaks (T_m) of neat PPR, HDPE, and TPU at 148.0 °C, 132.2 °C, and 175.8 °C, respectively. Two distinct melting temperatures of PPR and HDPE in the binary blend filament (P80E20T0) were separately detected at 147.8 °C and 130.7 °C which were very close to those of the virgin polymers, indicating the physical coexistence of both polymers. The incorporation of 20 wt % HDPE into the filament did not alter the melting temperature of the main PPR phase. However, a negligible change (about 2 °C) in T_m of the blended HDPE was found, compared to that of the neat HDPE. This observation rather agreed with the incident previously reported when HDPE was blended with PP homopolymer.[30] Furthermore, the blending of 30 wt % TPU into the PPR/HDPE binary blend did not further cause any changes in the melting temperatures of both PPR and HDPE, suggesting that the presence of TPU in P50E20T30 did not intervene the crystallization phases and perhaps crystallization of PPR and HDPE. A similar remark was disclosed in the blends of PP and TPU.[31] This was probably attributed to the difference in the polarity of the nonpolar polyolefins and the polar TPU; the phase separation between the polyolefins and TPU could then occur. As observed, the endothermic melting peak of the virgin TPU specimen at 175.8 °C was so tiny that it was barely detected in the DSC curve of P50E20T30 and was then not reported in Table 3.

Figure 4b reveals the exothermic crystallization peaks (T_c) of pristine PPR, HDPE, and TPU at 106.3 °C, 115.2 °C, and 100.8 °C, respectively. The blend of PPR and HDPE (P80E20T0) vividly exhibited two single crystallization peaks with T_c values of PPR and HDPE slightly deviated (2−4 °C) from those detected in the individual homopolymers (Table 3). The minimal increases in the crystallization temperatures of both polyolefins were likely associated with the well-known

https://doi.org/10.1021/acsomega.4c05502
ACS Omega 2024, 9, 35131−35143

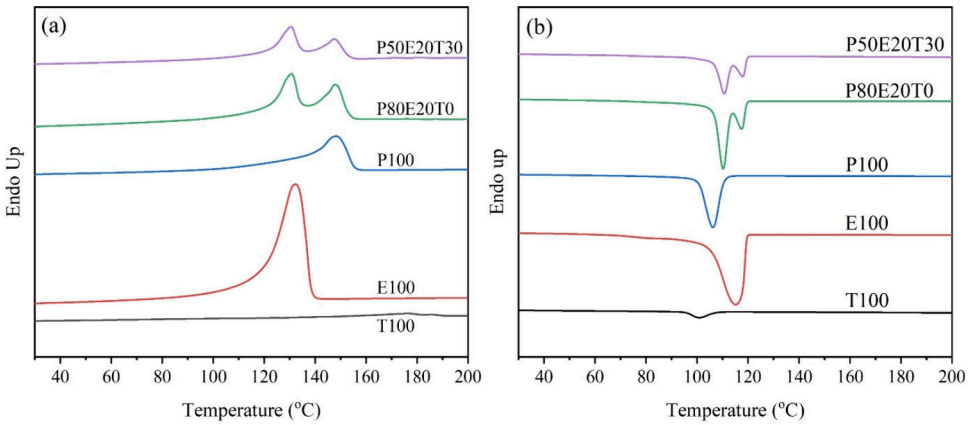

Figure 4. Differential scanning calorimetry thermograms of the PPR-based blend filaments and their parent polymers: (a) heating and (b) cooling cycles.

Table 3. Melting Temperatures (T_m), Crystallization Temperatures (T_c), Melting Enthalpy (ΔH_m), Crystallization Enthalpy (ΔH_c), and Degrees of Crystallinity ($X_{c,DSC}$) (%) of the PPR-Based Blend and Neat Polymer Samples Determined from the Endothermic Melting Peaks in their DSC Curves and Theoretical Degree of Crystallinity ($X_{c,theo,DSC}$) (%)

Sample codes	T_m (°C)[a]	T_c (°C)[a]	ΔH_m (J/g)	ΔH_c (J/g)	$X_{c,DSC}$ (%)[b]	$X_{c,theo,DSC}$ (%)[c]
P100	148.0	106.3	75.8	79.7	36.6	–
E100	132.2	115.2	188.6	193.1	64.4	–
T100	175.8	100.8	9.1	11.1	4.6	–
P80E20T0	147.8[a]/130.7[b]	110.2[a]/117.5[b]	109.9	110.7	49.0	42.2
P50E20T30	147.5[a]/130.5[b]	110.7[a]/117.8[b]	68.6	68.3	31.0	32.6

[a]Superscripts "a" and "b" indicate the measured melting temperatures of PPR and HDPE, respectively, in the blends. [b]Determined from the melting enthalpy of crystallization of each test sample using eq 2 in Section 2.4.1. [c]Calculated from eq 3 in Section 2.4.1.

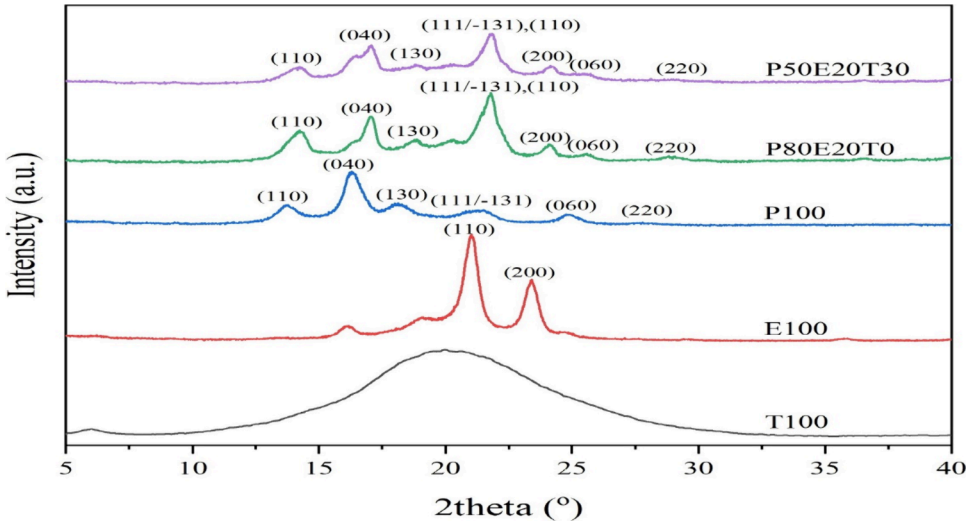

Figure 5. X-ray diffraction patterns of the FDM-fabricated PPR-based blend and the corresponding parent polymer specimens.

cocrystallization process where PPR and HDPE chains participated together in the development of crystals, suggesting a partially miscible behavior.[32] The incorporated HDPE probably acted as crystalline nuclei and subsequently facilitated the heterogeneous nucleating of the PPR macromolecule segments in the blend.[33] Seemingly, the integration of 30 wt % TPU into the PPR/HDPE blend did not further alter the crystallization temperatures of both PPR and HDPE in the ternary blend; a similar bimodal exothermic peak in the DSC curve was still spotted, indicating that TPU did not serve as a nucleating agent in the polyolefin matrices of P50E20T30. In addition, the crystallization peak of TPU blended at 30 wt % was not distinctly observed, owing to its relatively much lower crystallizability, and thus not reported in Table 3.

3.3. Crystallization and Crystalline Morphology.

3.3.1. Degree of Crystallinity. The percentages of crystallinity (X_c) (%) of the PPR-based blends were comparatively determined by DSC and XRD analyses with respect to those of the parent homopolymers. In DSC analysis, the current crystallinity ($X_{c,DSC}$) of each test sample was straightforwardly calculated from its melting enthalpy of crystallization, measured from the area of melting peak, with a use of eq 2. Meanwhile, the theoretical degree of crystallinity (%) of each blend specimen ($X_{c,theo,DSC}$) was comparatively calculated,

https://doi.org/10.1021/acsomega.4c05502
ACS Omega 2024, 9, 35131−35143

based on the $X_{c,DSC}$ value and weight fraction of each homopolymer blended, using eq 3. The $X_{c,DSC}$ values of the individual neat polymers and their blends are listed in Table 3. Along with the slightly earlier crystallization of PPR and HDPE in the blend sample, the experimentally determined percent crystallinity of this binary blend was apparently found to be somewhat higher than the theoretical value, about 7%, confirming that HDPE in the blend likely functioned as crystalline nuclei that later accelerated the nucleation of the PPR molecules. The $X_{c,DSC}$ value of the binary blend was expected to decrease when 30 wt % of a relatively lower crystallizable polymer, i.e., TPU, was added to the blend; nonetheless, the $X_{c,DSC}$ and $X_{c,theo,DSC}$ values of the ternary blend (P50E20T30) were not much different, positively supporting that TPU neither acted as a nucleating agent nor altered the crystalline phases of the polyolefins in the blend.

The crystalline phases and percentages of crystallinity of both P80E20T0 and P50E20T30 were further investigated by using XRD analysis. The FDM-fabricated specimens of these two filaments were examined in comparison to the discs of the parent polymers. As demonstrated in Figure 5, the broad diffraction band of the pure TPU specimen (T100) was intensely observed in the range of $2\theta = 5°-35°$, indicating that the polymer was nearly completely amorphous. This was rather agreeable with the DSC result stated above. On the other hand, the XRD pattern of the pristine PPR specimen (P100) revealed six distinct peaks at 2θ of 13.73°, 16.31°, 18.17°, 21.41°, 24.87°, and 27.69° belonging to the (110), (040), (130), (111/−131), (060), and (220) crystal planes, respectively;[34,35] this represented the α-monoclinic form of isotactic polypropylene. The orthorhombic crystal form of HDPE was pronouncedly perceived with the crystalline lattice planes of (110) and (200) at the 2θ values of 21.01° and 23.41°, respectively.[36] A PPR/HDPE combined crystalline pattern was apparently seen in the XRD pattern of P80E20T0; the broad and tiny crystalline peak of PPR at 2θ of 21.41° was, of course, hidden in the sharp characteristic peak of HDPE ((110) plane). This suggested that the crystal structure of PPR was not probably influenced by the presence of HDPE; the similar XRD results of PP/HDPE blends were also previously reported.[37] The XRD patterns of two PPR-based blends looked rather alike, except that the peak intensities of the PPR crystal planes, i.e., (110), (040), and (111/−131), marginally subsided owing to their decreased weight fraction when TPU was additionally incorporated. This was evidenced that the existence of TPU in P50E20T30 did not perturb the crystallizibilities of the polyolefins, which was pertinently agreed with the DSC result stated above and consistent with the phase behaviors of the TPU/isotactic PP blends reported previously.[30]

The degrees of crystallinity (X_c) of the PPR-based blend and parent polymer samples were also calculated from the ratios of the peak areas of the crystalline phase to the sum of the areas of the crystalline and amorphous phases in the XRD patterns. In addition, the crystallinity values of PPR and HDPE present in each PPR-based blend sample were concurrently quantified from the ratio of the peak areas of two nonoverlapping lattice planes, i.e., (110) of PPR to (200) of HDPE, with respect to the determined percent crystallinity of the blend sample on an assumption that TPU contributed no crystal lattices in the XRD pattern. In Table 4, the X_c results from XRD analysis are presented along with those obtained from the DSC study. Overall, it was noted that both characterization techniques

Table 4. Comparative Results of the Degrees of Crystallinity (X_c) (%) of the PPR-Based Blend and Neat Polymer Samples Determined by XRD and DSC Analyses

Sample codes	$X_{c,XRD}$ (%)[a]	$X_{c,DSC}$ (%)
P100	41.5	36.6
E100	57.4	64.4
T100	–	4.6
P80E20T0	46.6 (37.2[a]/9.4[b])	49.0
P50E20T30	40.1 (27.9[a]/12.3[b])	31.0

[a]Superscripts "a" and "b" indicate the X_c values of PPR and HDPE, respectively, present in each blend, measured from the ratio of the peak areas of (110) to (200), with respect to the determined percent crystallinity of each blend sample.

provided the results in a similar trend, where the X_c value of the neat PPR material was lower than that of the pure HDPE material, and the elastomeric TPU used in this study was almost absolutely noncrystalline. Hence, the X_c value of the PPR-based blend material was perceptibly decreased when TPU was blended. However, the X_c values of the PPR/HDPE blend, measured by both DSC and XRD, were found to be slightly higher than the theoretical values (using eq 3); this was likely due to the cocrystallization phenomenon of propylene and ethylene macromolecules.[38] This was also confirmed by the crystallinity values of PPR (37.2%) and HDPE (9.4%) found in P80E20T0, which was measured directly from the peak areas of (110) and (200) with respect to the $X_{c,XRD}$ value (46.6%) of the blend material. Theoretically, using eq 3, the $X_{c,XRD}$ values of these two polyolefins should have been 33.2% and 11.5%, respectively. In the presence of HDPE, PPR happened to crystallize more readily, i.e., at a slightly higher T_c (Table 3) with somewhat greater crystallinity, as HDPE might perhaps act as crystalline nuclei for PPR crystallization. Noticeably, the determined $X_{c,XRD}$ value of PPR in the P50E20T30 blend sample sharply dropped from 37.2% to 27.9%; this number was, however, still greater than the theoretical value (20.7%). On the other hand, the measured $X_{c,XRD}$ value of HDPE in the blend somewhat increased from 9.4% to 12.3%. This was, however, not much different from the theoretical number (11.5%). As a result, it was likely to conclude that the presence of TPU in the blend barely affected the crystallization of HDPE in the material; the experimentally determined crystallinity of HDPE remained rather close to the theoretical value found in each PPR-based blend.

3.3.2. Isothermal Crystallization Behavior. The complex crystallization behaviors of the individual polymer components in the ternary blends were further investigated using hot stage polarized light optical microscopy (PLOM). All test materials were initially heated at 240 °C for 4 min before being cooled to varied temperatures, in which the isothermal crystal formations of PPR, HDPE, and TPU in the neat and blend samples were subsequently monitored and micrographed. According to the T_m and T_c values observed by DSC (Table 3), the molten neat PPR, HDPE, and TPU were cooled to 110 °C, 120 °C, and 150 °C, respectively, and held at those temperatures for 10 min before being imaged. Figure 6 displays PLOM micrographs of the spherulitic morphologies of P100, E100, and T100. The large spherulites of the pristine PPR sample were well-developed with clear boundaries, featuring a characteristic Maltese cross-extinction pattern (flowerlike spherulites) (Figure 6a),[37] whereas the relatively much smaller crystals of the pure HDPE specimen were more densely

https://doi.org/10.1021/acsomega.4c05502
ACS Omega 2024, 9, 35131−35143

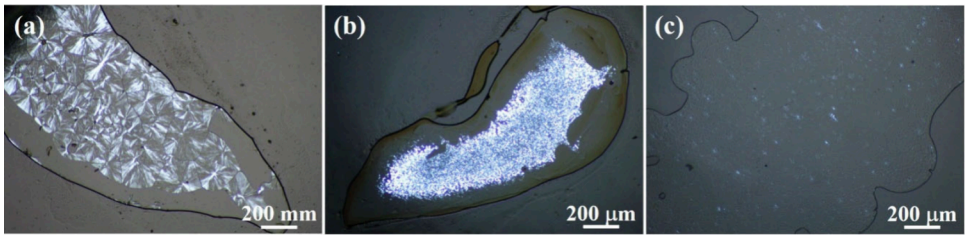

Figure 6. Polarized light optical micrographs of (a) P100, (b) E100, and (c) T100 being held isothermally at 110 °C, 120 °C, and 150 °C, respectively, for 10 min.

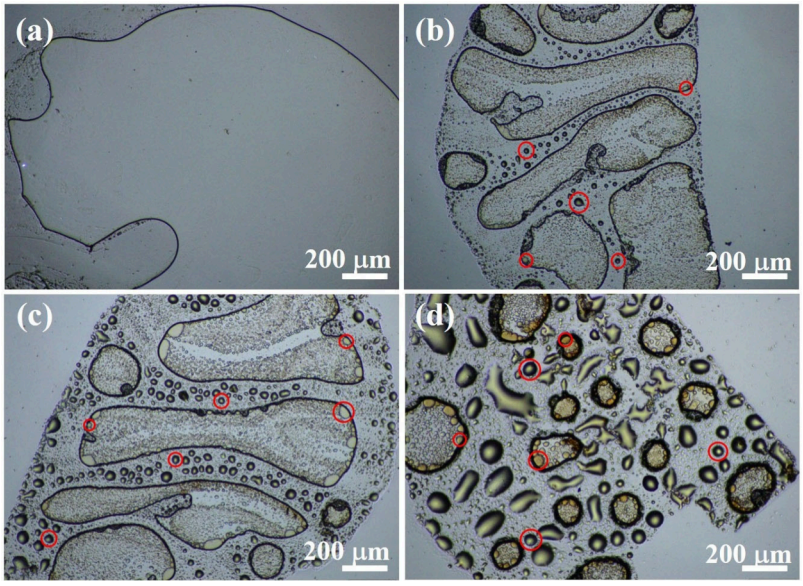

Figure 7. Polarized light optical micrographs of (a) P80E20T0, (b) P70E20T10, (c) P60E20T20, and (d) P50E20T30 being held isothermally at 170 °C for 5 min.

formed (Figure 6b). In contrast, few spherulites were intermittently found in the pure TPU material (Figure 6c), indicating its low crystallinity, as evidenced by both the DSC and XRD results mentioned previously.

Figure 7 displays the PLOM images of the PPR-based filament samples containing various amounts of TPU, i.e., 0, 10, 20, and 30 wt %, taken after the materials were isothermally held at 170 °C for 5 min. As expected, the micrograph of the molten P80E20T0 specimen appeared totally clear, with no phase separation manifestly detected (Figure 7a). When TPU was integrated into the PPR/HDPE blend, the phase-separated structures of the molten ternary blend samples were visibly formed (Figure 7b–d). The combined phases of PPR and HDPE were now observed as aggregates encircled by clear dark rings, whereas the TPU phase was found in a droplet form (indicated by the red circles). Interestingly, although most of the TPU droplets were located outside (surrounding) the PPR/HDPE molten aggregates, there existed few TPU droplets inside the polyolefin aggregates, specifically near the dark circles. The sizes of the PPR/HDPE aggregates and TPU droplets were seemingly governed by the amount of TPU blended. The higher the content of TPU added, the smaller the PPR/HDPE aggregates, but the larger the TPU droplets, found. As a result, the TPU phase of P50E20T30 became most homogeneously dispersed throughout the entire blend morphology. Furthermore, the number of TPU droplets embedded in the aggregate phase was more markedly perceived. This suggested that the morphology of the molten PPR/HDPE/TPU ternary blend was not completely phase-separated.

To investigate the crystallization behaviors of PPR and HDPE in the blends with and without the nearly noncrystalline TPU polymer, the microtome slices of both P80E20T0 and P60E20T20 filaments were individually heated to 240 °C, followed by gradual cooling to isothermal temperatures of 170 °C, 160 °C, 150 °C, 120 °C, and 110 °C, respectively, with various isothermal holding times, i.e., 5, 10, 20, and 60 min. The PLOM images of each PPR-based blend sample isothermally held at 170 °C, 160 °C, and 150 °C for 5 min looked rather alike (similar to those shown in Figure 7a (for P80E20T0) and Figure 7c (for P50E20T30)). According to the low-volume incorporation, a few HDPE crystals were detected in the binary blend but hardly observed in the ternary blend, at the isothermal temperature/time of 120 °C/20 min, as illustrated in Figure 8. The irregular distribution of the HDPE crystallinephase inside the polymer matrix firmly suggested that the PPR/HDPE blend was incompatible. After being cooled to 110 °C and held still for 20 min, PPR crystals were markedly found in the binary blend; however, the structure of PPR spherulites appeared small, incomplete, and needle-like. This phenomenon was absolutely attributed to the mutual restriction of crystallization of the two polymer components.[39] At a prolonged isothermal holding time (60 min), the continuous growth of PPR spherulites was evidently noted. It was difficult to differentiate the HDPE crystals from the relatively larger PPR spherulites. Noticeably, the PPR

https://doi.org/10.1021/acsomega.4c05502
ACS Omega 2024, 9, 35131−35143

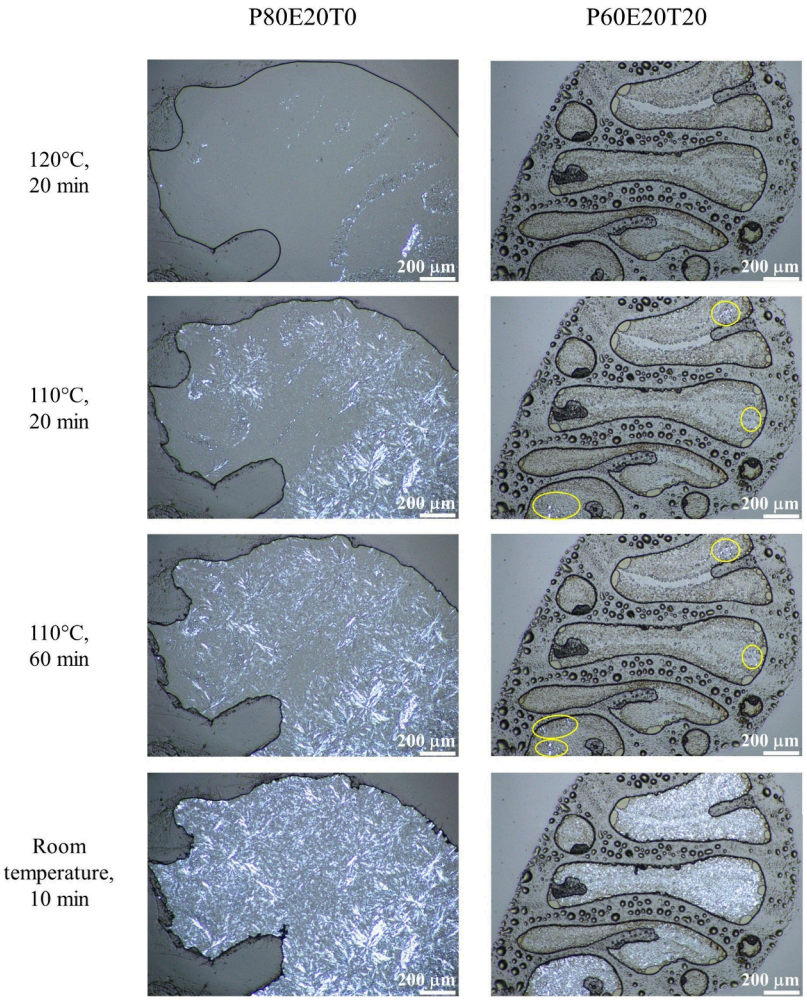

Figure 8. Polarized light optical micrographs of P80E20T0 (left) and P60E20T20 (right) being held isothermally at 120 °C for 20 min, 110 °C for 20 and 60 min, and room temperature for 10 min.

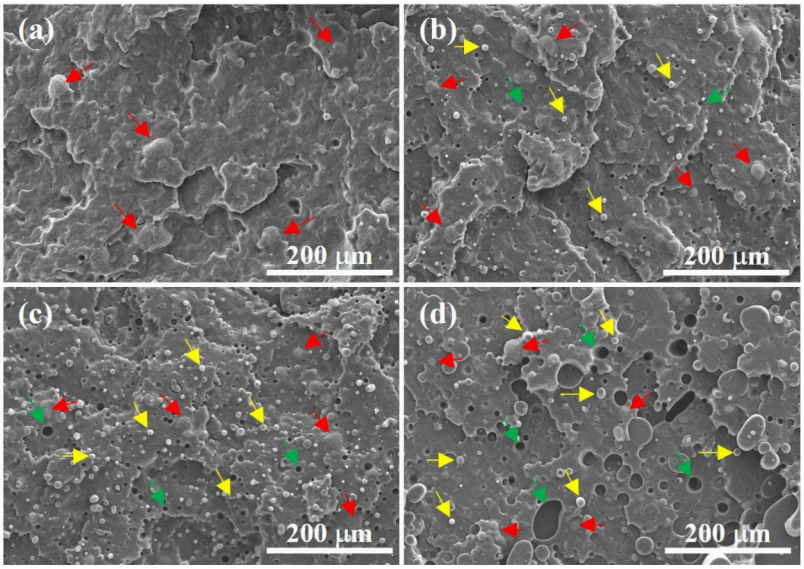

Figure 9. SEM images of the cryo-fractured surfaces of (a) P80E20T0, (b) P70E20T10, (c) P60E20T20, and (d) P50E20T30 filaments. Red and yellow arrows indicate the HDPE and TPU domains, respectively, in the PPR filament matrix. Green arrows point to the voids formed in the filament matrices.

spherulites formed more densely where HDPE were located, implying that HDPE likely acted as crystallization nuclei in the crystallization of the adjacent PPR molecules. This also possibly led to a reduction in the size of PPR crystals.

https://doi.org/10.1021/acsomega.4c05502
ACS Omega 2024, 9, 35131−35143

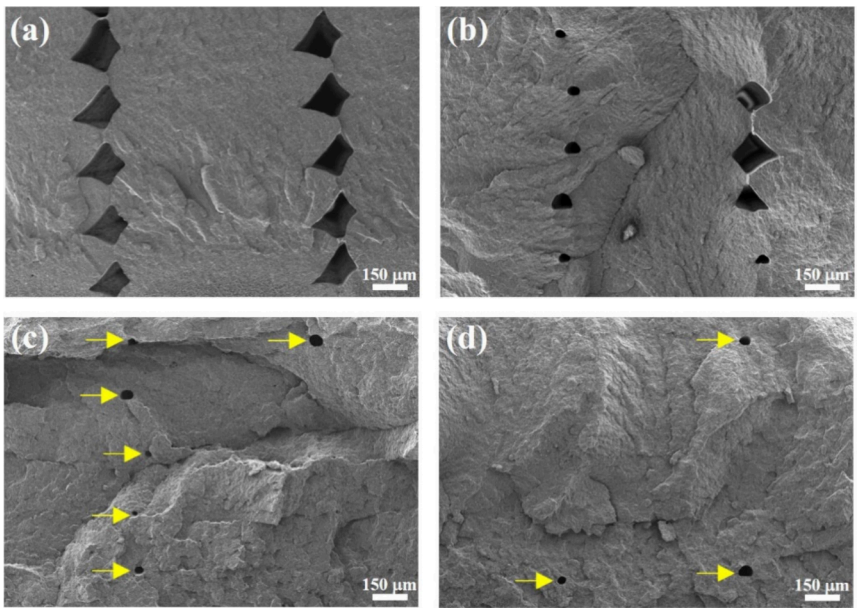

Figure 10. SEM images of the cryo-fractured surfaces of the as-printed specimens fabricated from (a) P80E20T0, (b) P70E20T10, (c) P60E20T20, and (d) P50E20T30 filaments. Yellow arrows indicate the voids generated in the deposited adjacent rasters.

Meanwhile, at 110 °C, the crystallization behavior of the ternary blend still exhibited phase-separated morphologies between the polyolefin matrix and TPU phase (similar to that described above) with minimal detections of crystals in the micrographs of P60E20T20 isothermally held for 20 and 60 min (indicated by yellow circles). After the materials were cooled to room temperature for 10 min, the PLOM micrographs of the PPR-based blends revealed the significantly increased numbers of crystals in both materials, indicating the complete crystallization processes of both PPR and HDPE. Nonetheless, the crystal morphology observed in the ternary blend was considerably different from that seen in the binary blend. This suggested that the presence of TPU, a polar material, in the nonpolar PPR main matrix of the blend explicitly restricted the crystallization of PPR, which resulted in not only the size of spherulites being reduced but also the growth rate being slowed down. The TPU phase limited the diffusion movements and conformational transitions of both PPR and HDPE molecules during their crystallization and growths.[40]

3.4. Internal Surface Morphology. The cryo-fractured surfaces of the PPR/HDPE/TPU blend filaments were comparatively assessed by SEM. As revealed in Figure 9a, the two-phase morphology of the PPR/HDPE blend filament (P80E20T0) was observed with a random dispersion of the spherical HDPE domain (indicated by red arrows) in the continuous PPR matrix. Principally, PPR and HDPE are nonpolar whereas TPU is polar. Thus, the differences in polarity and interfacial tension of the materials made the ternary blends incompatible.[41] As shown in Figure 9b–d, the internal surface homogeneity of the blend filaments was drastically reduced when an increasing amount of TPU was integrated. In addition, the number and size of TPU droplets (pointed by yellow arrows) became larger with greater content of TPU incorporated into the blends. The observed phase-separated morphology of the blend filament specimens was in good agreement with that detected in the PLOM study mentioned above. Upon filament processing, the coalescence of TPU droplets could partially occur, particularly when a high content of TPU was blended, causing deteriorated surface roughness and even generating voids (indicated by green arrows). Moreover, once the filaments were fractured, the TPU particles could be partly pulled out, causing some voids in the filament matrices, because of the poor interfacial adhesion between TPU and PPR/HDPE phases.[42]

The interlayer bonding integrity of the FDM-printed specimens with a raster angle of 0° was assessed by SEM. As seen in Figure 10, the internal voids were observed in all 3D-printed specimens, which was primarily caused by thermal shrinkage of the materials surrounding the gaps between adjacent rasters during cooling. Seemingly, the cross-sectional surface of the specimen fabricated from the binary blend filament (P80E20T0) exhibited the hugest size of the internal voids in every raster gap. Significant decreases in both the size and number of internal voids in the fractured-surfaces of the 3D specimens were noticed as the amount of blended TPU increased, as illustrated in Figure 10b–d. This was principally caused by the enhanced layer interfusion together with the lessened shrinkages of the materials upon cooling. Since TPU had a lower thermal shrinkage than those of PPR and HDPE,[43] the incorporation of TPU into the PPR/HDPE blend filaments not only reduced the shrinkages of the printed materials but also helped improve the adhesion between adjacent rasters, yielding better interlayer bonding integrity.

3.5. Warpage Deformation. Generally, warpage of FDM-printed specimens caused by the volumetric shrinkage during the cooling process of the materials is a significant challenging printing obstacle, remarkably in the printing of semicrystalline polymer filaments.[44] Warpage distortion typically occurs along the edge of a fabricated object. In this study, the warpage deformation of each as-printed object was determined in terms of specific warpage (W_{sp}) which was defined as the average absolute warpage divided by the maximum height of a printed specimen (Figure 2 and eq 4). The 3D specimens for warpage test were printed layer-by-layer by using the printing parameters listed in Table 2 without adhesive or fixation spray applied on the build platform, into a rectangular shape (10 mm width × 80 mm length × 4 mm thickness) designed

https://doi.org/10.1021/acsomega.4c05502
ACS Omega 2024, 9, 35131−35143

Table 5. Specific Warpage (%) of the 3D As-Printed Specimens Fabricated from the PPR-Based Blend Filaments

Sample codes	Absolute warpage (W_{abs}) (mm)			H_{max} (mm)	Specific warpage (W_{sp}) (%)[a]
	Left	Right	Average		
P80E20T0	1.17 ± 0.08	1.42 ± 0.12	1.30 ± 0.10	4.06 ± 0.00	31.90 ± 2.46[a]
P70E20T10	0.76 ± 0.25	0.88 ± 0.30	0.82 ± 0.07	4.31 ± 0.16	18.95 ± 1.05[b]
P60E20T20	0.53 ± 0.17	0.51 ± 0.28	0.52 ± 0.20	4.10 ± 0.33	12.52 ± 3.65[c]
P50E20T30	0.31 ± 0.13	0.36 ± 0.10	0.33 ± 0.11	3.99 ± 0.09	8.31 ± 2.49[c]

[a]The data are expressed as the mean ± SD (n = 3). Different superscript letters (a, b, and c) indicate significant differences between four samples at $p < 0.05$, analyzed by one-way ANOVA with Duncan test.

using a CAD software program (SolidWorks). The absolute warpage at the left and right corners ($W_{abs,Left}$ and $W_{abs,Right}$) and the maximum height (H_{max}) of each as-printed specimen were promptly determined from its photograph (Figure S1) using ImageJ software and subsequently used for the calculation of the corresponding specific warpage (W_{sp}).

As revealed in Table 5, the 3D specimen fabricated from the nonpolar, semicrystalline PPR/HDPE blend filament (P80E20T0) possessed the highest W_{sp} value (31.90 ± 2.46%) with unbalanced warpage deformation at the left and right corners of the object. Incorporating TPU into the PPR/HDPE blend filament could drastically reduce the W_{sp} value by 41%, 61%, and 74% when the 3D articles were fabricated from P70E20T10, P60E20T20, and P50E20T30 blend filaments, respectively. Blending TPU, a nearly noncrystalline polymer, into a semicrystalline PPR/HDPE blend absolutely lowered the overall degree of crystallinity of the resulting ternary blend; the higher the amount of TPU added, the greater the reduction in crystallinity of the blended material resulted (as evidenced by both DSC and XRD results mentioned above). Furthermore, TPU is a thermoplastic that can be processed at a relatively lower extrusion temperature. Also, it has a relatively lower coefficient of thermal expansion compared to those of PPR and HDPE, which hence helps reduce internal stresses during cooling. As revealed in Figure 7, though most of TPU droplets were located apart from the PPR/HDPE mixed phase of the PPR-based blend filaments, some of them fused into the polyolefin binary phase. Taken altogether, the least warpage deformation of the as-printed articles was unquestionably found in the specimen printed from P50E20T30. This was in good accordance with our previous study on minimizing warpage deformation of the 3D articles fabricated from the ABS/TPU blend filaments.[45]

3.6. Mechanical Properties. The flexural strength and moduli of the 3D specimens (XY orientation) individually printed from the four different PPR-based blend filaments were comparatively evaluated at room temperature by using a universal testing machine with a 10 kN load cell. As demonstrated in Figure 11, the 3D-printed PPR/HDPE blend specimen exhibited the highest flexural strength and modulus owing to its inherent rigidity. Integrating TPU into the PPR/HDPE blend filament significantly lowered the flexural strength of the fabricated objects by approximately 2.9%, 14.8%, and 25.7% when the 3D articles were fabricated from P70E20T10, P60E20T20, and P50E20T30, respectively. In contrast, the flexural moduli of the fabricated objects gradually dropped with increasing content of TPU blended in the filaments. The decrease in strength was accompanied by a notable increase in the flexibility of the 3D ternary blend samples due to the presence of the flexible TPU component. This observation was consistent with a previous study that

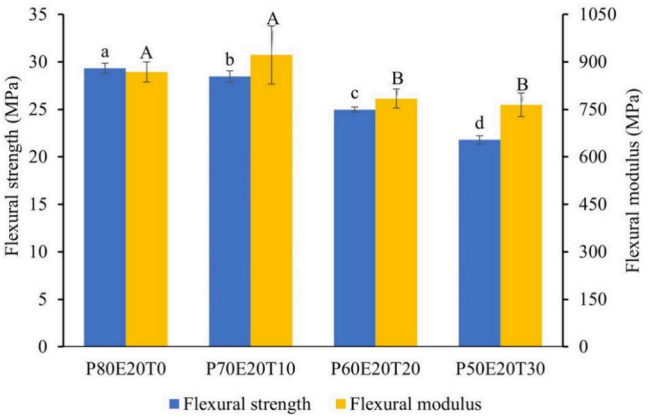

Figure 11. Flexural strength and moduli of the as-printed specimens separately fabricated from the different PPR-based blend filaments. The data are expressed as the mean ± SD (n = 5), and the different capital (A and B) and small (a, b, c, and d) letters indicate significant differences at $p < 0.05$, analyzed by one-way ANOVA with Duncan test.

demonstrated the stiffness reduction of materials when TPU was incorporated into the PP matrix.[46]

CONCLUSIONS

In this work, the preparation and properties of newly developed PPR/HDPE/TPU ternary blend filaments for FDM printing were reported, along with the evaluated quality and performance of the corresponding as-printed specimens. The surface morphology of the PPR-based ternary blends was not entirely phase-separated. Although the incorporation of nearly noncrystalline flexible TPU into the ternary blends decreased the sizes and growth rates of the polyolefin crystals, it scarcely affected the crystallizability of each semicrystalline polymer. In addition, both warpage deformation and interlayer bonding of the FDM-fabricated articles were increasingly improved as the TPU content was raised, despite the fairly deterioration of mechanical performance of the 3D-printed materials. Ultimately, the findings suggested that the PPR/HDPE/TPU ternary blend filament with the well-tuned blend composition, i.e., P50E20T30, had a promising potential use as an FDM filament feedstock.

ASSOCIATED CONTENT

Supporting Information

The Supporting Information is available free of charge at https://pubs.acs.org/doi/10.1021/acsomega.4c05502.

The average filament diameters of the 3D printing PPR-based blend filaments and digital photographs of warpage deformation of the 3D specimens printed from the different PPR-based blend filaments (PDF)

https://doi.org/10.1021/acsomega.4c05502
ACS Omega 2024, 9, 35131−35143

AUTHOR INFORMATION

Corresponding Authors

Wanida Janvikul − *Biofunctional Materials and Devices Research Group, National Metal and Materials Technology Center, National Science and Technology Development Agency, Khlong Luang, Pathum Thani 12120, Thailand;* orcid.org/0000-0002-2560-0075; Email: wanidaj@mtec.or.th

Boonlom Thavornyutikarn − *Biofunctional Materials and Devices Research Group, National Metal and Materials Technology Center, National Science and Technology Development Agency, Khlong Luang, Pathum Thani 12120, Thailand;* orcid.org/0000-0002-9814-0065; Email: boonlomt@mtec.or.th

Authors

Wasana Kosorn − *Biofunctional Materials and Devices Research Group, National Metal and Materials Technology Center, National Science and Technology Development Agency, Khlong Luang, Pathum Thani 12120, Thailand*

Pornchanok Pichaipanich − *Biofunctional Materials and Devices Research Group, National Metal and Materials Technology Center, National Science and Technology Development Agency, Khlong Luang, Pathum Thani 12120, Thailand*

Phansiri Suktha − *Biofunctional Materials and Devices Research Group, National Metal and Materials Technology Center, National Science and Technology Development Agency, Khlong Luang, Pathum Thani 12120, Thailand*

Nutdanai Nampichai − *Biofunctional Materials and Devices Research Group, National Metal and Materials Technology Center, National Science and Technology Development Agency, Khlong Luang, Pathum Thani 12120, Thailand*

Complete contact information is available at: https://pubs.acs.org/10.1021/acsomega.4c05502

Author Contributions

#W.K. and P.P. equally contributed to this work.

Author Contributions

Wasana Kosorn and Pornchanok Pichaipanich: Conceptualization, Methodology, Formal analysis, Investigation, Writing of the original draft. Phansiri Suktha: Methodology, Formal analysis, Investigation. Nutdanai Nampichai: Methodology, Formal analysis. Boonlom Thavornyutikarn: Funding acquisition, Co-supervision, Writing of the original draft, Review. Wanida Janvikul: Funding acquisition, Supervision, Manuscript composition, Review and Editing. All authors have read and agreed to the published version of the manuscript.

Notes

The authors declare no competing financial interest.

ACKNOWLEDGMENTS

The present study was financially supported by the National Research Council of Thailand (NRCT) under grant number N34A660023 funded to the National Science and Technology Development Agency, Thailand (Project Code: P22-51373). Additionally, this research received a human resource funding grant from the NSRF via the Program Management Unit for Human Resources & Institutional Development, Research and Innovation (PMU-B) (grant number B13F660064).

REFERENCES

(1) Cicala, G.; Latteri, A.; Del Curto, B.; Lo Russo, A.; Recca, G.; Fare, S. Engineering Thermoplastics for Additive Manufacturing: A Critical Perspective with Experimental Evidence to Support Functional Applications. *J. Appl. Biomater. Funct. Mater.* **2017**, *15* (1), 10−18.

(2) Sathies, T.; Senthil, P.; Anoop, M. S. A review on advancements in applications of fused deposition modelling process. *Rapid Prototyp. J.* **2020**, *26* (4), 669−687.

(3) Rahim, T. N. A. T.; Abdullah, A. M.; Md Akil, H. Recent developments in fused deposition modeling-based 3D printing of polymers and their composites. *Polym. Rev.* **2019**, *59* (4), 589−624.

(4) Galli, P.; Vecellio, G. Technology: driving force behind innovation and growth of polyolefins. *Prog. Polym. Sci.* **2001**, *26* (8), 1287−1336.

(5) Carneiro, O. S.; Silva, A.; Gomes, R. Fused deposition modeling with polypropylene. *Mater. Des.* **2015**, *83*, 768−776.

(6) Hertle, S.; Drexler, M.; Drummer, D. Additive manufacturing of poly (propylene) by means of melt extrusion. *Macromol. Mater. Eng.* **2016**, *301* (12), 1482−1493.

(7) Leng, J.; Gu, X.; Hong, R.; Zhang, J. Tailored crystalline structure and enhanced impact strength of isotactic polypropylene/high-density polyethylene blend by controlling the printing speed of fused filament fabrication. *J. Mater. Sci.* **2020**, *55*, 14058−14073.

(8) Vaes, D.; Van Puyvelde, P. Semi-crystalline feedstock for filament-based 3D printing of polymers. *Prog. Polym. Sci.* **2021**, *118*, 101411.

(9) Jin, M.; Neuber, C.; Schmidt, H.-W. Tailoring polypropylene for extrusion-based additive manufacturing. *Addit. Manuf.* **2020**, *33*, 101101.

(10) Spoerk, M.; Holzer, C.; Gonzalez-Gutierrez, J. Material extrusion-based additive manufacturing of polypropylene: A review on how to improve dimensional inaccuracy and warpage. *J. Appl. Polym. Sci.* **2020**, *137* (12), 48545.

(11) Spoerk, M.; Gonzalez-Gutierrez, J.; Sapkota, J.; Schuschnigg, S.; Holzer, C. Effect of the printing bed temperature on the adhesion of parts produced by fused filament fabrication. *Plast. Rubber. Compos.* **2018**, *47* (1), 17−24.

(12) Paxton, N. C.; Allenby, M. C.; Lewis, P. M.; Woodruff, M. A. Biomedical applications of polyethylene. *Eur. Polym. J.* **2019**, *118*, 412−428.

(13) Schirmeister, C. G.; Hees, T.; Licht, E. H.; Mülhaupt, R. 3D printing of high density polyethylene by fused filament fabrication. *Addit Manuf.* **2019**, *28*, 152−159.

(14) Harris, M.; Potgieter, J.; Ray, S.; Archer, R.; Arif, K. M. Preparation and characterization of thermally stable ABS/HDPE blend for fused filament fabrication. *Mater. Manuf. Process.* **2020**, *35* (2), 230−240.

(15) Chatkunakasem, P.; Luangjuntawong, P.; Pongwisuthiruchte, A.; Aumnate, C.; Potiyaraj, P. Tuning of HDPE properties for 3D printing. *Key. Eng. Mater.* **2018**, *773*, 67−71.

(16) Verma, N.; Awasthi, P.; Gupta, A.; Banerjee, S. S. Fused Deposition Modeling of Polyolefins: Challenges and Opportunities. *Macromol. Mater. Eng.* **2023**, *308* (1), 2200421.

(17) Peng, X.; He, H.; Jia, Y.; Liu, H.; Geng, Y.; Huang, B.; Luo, C. Shape memory effect of three-dimensional printed products based on polypropylene/nylon 6 alloy. *J. Mater. Sci.* **2019**, *54* (12), 9235−9246.

(18) Slonov, A.; Musov, I.; Zhansitov, A.; Khashirov, A.; Tlupov, A.; Musov, K.; Rzhevskaya, E.; Fomicheva, I.; Potapov, A.; Khashirova, S. Investigation of the Properties of Polyethylene and Ethylene-Vinyl Acetate Copolymer Blends for 3D Printing Applications. *Polymers* **2023**, *15* (20), 4129.

(19) Schirmeister, C. G.; Schächtele, S.; Keßler, Y.; Hees, T.; Köhler, R.; Schmitz, K.; Licht, E. H.; Muelhaupt, R. Low warpage nanophase-separated polypropylene/olefinic elastomer reactor blend composites with digitally tuned glass fiber orientation by extrusion-based additive manufacturing. *ACS Appl. Polym. Mater.* **2021**, *3* (4), 2070−2081.

(20) Ho, Q. B.; Kontopoulou, M. Improving the adhesion and properties in the material extrusion of polypropylene by blending with a polyolefin elastomer. *Addit. Manuf.* **2022**, *55*, 102818.
(21) Banerjee, S. S.; Burbine, S.; Kodihalli Shivaprakash, N.; Mead, J. 3D-printable PP/SEBS thermoplastic elastomeric blends: Preparation and properties. *Polymers* **2019**, *11* (2), 347.
(22) Ciobanu, R. C.; Schreiner, C.; Aradoaei, M.; Hitruc, G. E.; Rusu, B. G.; Aflori, M. Characteristics of Composite Materials of the Type: TPU/PP/BaTiO(3) Powder for 3D Printing Applications. *Polymers* **2023**, *15* (1), 73.
(23) Xiao, X.; Chevali, V. S.; Song, P.; He, D.; Wang, H. Polylactide/hemp hurd biocomposites as sustainable 3D printing feedstock. *Compos. Sci. Technol.* **2019**, *184*, 107887.
(24) Verma, P.; Choudhary, V. Polypropylene random copolymer/MWCNT nanocomposites: isothermal crystallization kinetics, structural, and morphological interpretations. *J. Appl. Polym. Sci.* **2015**, *132* (13). DOI: 10.1002/app.41734
(25) Tarani, E.; Arvanitidis, I.; Christofilos, D.; Bikiaris, D. N.; Chrissafis, K.; Vourlias, G. Calculation of the degree of crystallinity of HDPE/GNPs nanocomposites by using various experimental techniques: A comparative study. *J. Mater. Sci.* **2023**, *58* (4), 1621−1639.
(26) de Avila Bockorny, G.; Forte, M. M. C.; Stamboroski, S.; Noeske, M.; Keil, A.; Leite Cavalcanti, W. Modifying a thermoplastic polyurethane for improving the bonding performance in an adhesive technical process. *Appl. Adhes. Sci.* **2016**, *4* (1). DOI: 10.1186/s40563-016-0060-x
(27) Bachhar, N.; Gudadhe, A.; Kumar, A.; Andrade, P.; Kumaraswamy, G. 3D printing of semicrystalline polypropylene: towards eliminating warpage of printed objects. *Bull. Mater. Sci.* **2020**, *43*, 1−8.
(28) ISO 178:2023. *Plastics-Determination of flexural properties*; The British Standards Institution: 2023; pp 1−28.
(29) Ponsar, H.; Wiedey, R.; Quodbach, J. Hot-Melt Extrusion Process Fluctuations and their Impact on Critical Quality Attributes of Filaments and 3D-printed Dosage Forms. *Pharmaceutics* **2020**, *12* (6), 511.
(30) Sutar, H.; Sahoo, P. C.; Sahu, P. S.; Sahoo, S.; Murmu, R.; Swain, S.; Mishra, S. C. Mechanical, Thermal and Crystallization Properties of Polypropylene (PP) Reinforced Composites with High Density Polyethylene (HDPE) as Matrix. *Materials Sciences and Applications* **2018**, *09* (05), 502−515.
(31) Lin, T.; Lou, C.-W.; Lin, J.-H. The Effects of Thermoplastic Polyurethane on the Structure and Mechanical Properties of Modified Polypropylene Blends. *Appl. Sci.* **2017**, *7* (12), 1254.
(32) Aumnate, C.; Rudolph, N.; Sarmadi, M. Recycling of Polypropylene/Polyethylene Blends: Effect of Chain Structure on the Crystallization Behaviors. *Polymers* **2019**, *11* (9), 1456.
(33) Shankar, G. K.; Raju, K.; Ramkumar, M.; Tamilarasy, T. Improving and Analysis of Material Characteristics of Polypropylene by Blending with High Density Polyethylene. *International Journal of Science Technology & Engineering* **2016**, *2* (10), 1106−1111.
(34) Lanyi, F. J. Modification of Interfacial Properties of Polypropylene Fibers using Hydrophilic Melt Additives - Interactions with Crystallization; FAU University Press, FAU University Press: 2020.
(35) Liu, J.; Liu, J. Characterization of maleic anhydride/styrene melt-grafted random copolypropylene and its impact on crystallization and mechanical properties of isotactic polypropylene. *Polym. Bull.* **2019**, *76* (9), 4369−4387.
(36) Wang, F.; Liu, L.; Xue, P.; Jia, M. Crystal Structure Evolution of UHMWPE/HDPE Blend Fibers Prepared by Melt Spinning. *Polymers* **2017**, *9* (3), 96.
(37) Lin, J. H.; Pan, Y. J.; Liu, C. F.; Huang, C. L.; Hsieh, C. T.; Chen, C. K.; Lin, Z. I.; Lou, C. W. Preparation and Compatibility Evaluation of Polypropylene/High Density Polyethylene Polyblends. *Materials* **2015**, *8* (12), 8850−8859.
(38) Carmeli, E.; Kandioller, G.; Gahleitner, M.; Müller, A. J.; Tranchida, D.; Cavallo, D. Continuous Cooling Curve Diagrams of Isotactic-Polypropylene/Polyethylene Blends: Mutual Nucleating Effects under Fast Cooling Conditions. *Macromolecules* **2021**, *54* (10), 4834−4846.
(39) Wang, J.; Yang, L.; Li, X. In Situ Compatibilization of Isotactic Polypropylene and High-Density Polyethylene by a Melt Cobranching Reaction. *J. Polym. Environ.* **2022**, *30*, 1127−1140.
(40) Jia, S.; Qu, J.; Liu, W.; Wu, C.; Chen, R.; Zhai, S.; Huang, Z. Thermoplastic polyurethane/polypropylene blends based on novel vane extruder: A study of morphology and mechanical properties. *Polym. Eng. Sci.* **2014**, *54* (3), 716−724.
(41) Lin, T. A.; Limin, B.; Lin, M.-C.; Lin, J.-Y.; Lou, C.-W.; Lin, J.-H. Impact-resistant polypropylene/thermoplastic polyurethane blends: compatible effects of maleic anhydride on thermal degradation properties and crystallization behaviors. *J. Mater. Res. Technol.* **2019**, *8* (4), 3389−3398.
(42) Lin, W.; He, Y.; Qu, J. P. Super-Tough and Highly-Ductile Poly(l-lactic acid)/Thermoplastic Polyurethane/Epoxide-Containing Ethylene Copolymer Blends Prepared by Reactive Blending. *Macromol. Mater. Eng.* **2019**, *304* (6). DOI: 10.1002/mame.201900020
(43) Goff, J.; Whelan, T.; DeLaney, D. The Dynisco Extrusion Processors Handbook, 2nd ed.; Dynisco Inc: MA, 2000; pp 50−51.
(44) Schirmeister, C. G.; Schächtele, S.; Keßler, Y.; Hees, T.; Köhler, R.; Schmitz, K.; Licht, E. H.; Muelhaupt, R. Low Warpage Nanophase-Separated Polypropylene/Olefinic Elastomer Reactor Blend Composites with Digitally Tuned Glass Fiber Orientation by Extrusion-Based Additive Manufacturing. *ACS Appl. Polym. Mater.* **2021**, *3* (4), 2070−2081.
(45) Diederichs, E. V.; Picard, M. C.; Chang, B. P.; Misra, M.; Mielewski, D. F.; Mohanty, A. K. Strategy To Improve Printability of Renewable Resource-Based Engineering Plastic Tailored for FDM Applications. *ACS Omega.* **2019**, *4* (23), 20297−20307.
(46) Jaruttrakool, R.; Tanpichai, S.; Pentrakoon, D.; Potiyaraj, P. Reactive Blending of Thermoplastic Polyurethane and Polypropylene. *Int. Polym. Process.* **2010**, *25* (5), 327−333.

https://doi.org/10.1021/acsomega.4c05502
ACS Omega 2024, 9, 35131−35143